ELSEVIER

Dual steady solutions in natural convection between horizontal concentric cylinders

Joo-Sik Yoo
Department of Mechanical Engineering Education, Andong National University, Andong, Kyungpuk, Korea

Dual steady solutions in natural convection in an annulus between two horizontal concentric cylinders are numerically investigated for a fluid of Prandtl number 0.7. It is found that, when the Rayleigh number based on the gap width exceeds a certain critical value, dual steady two-dimensional (2-D) flows can be realized: one being the crescent-shaped eddy flow commonly observed and the other the flow consisting of two counter-rotating eddies and their mirror images. The critical Rayleigh number decreases as the inverse relative gap width increases. © *1996 by Elsevier Science Inc.*

Keywords: natural convection; dual solutions; counter-rotating eddies

Introduction

Natural convection in a horizontal concentric cylindrical annuls kept at constant surface temperatures has been received much attention because of theoretical interest and wide engineering applications, such as thermal energy storage systems, cooling of electronic components, and transmission cables. A comprehensive review of steady two-dimensional (2-D) convection was presented in the work of Kuehn and Goldstein (1976), in which experimental and numerical studies were performed to determine velocity and temperature distributions and local heat transfer coefficients for convective flows of air and water within a horizontal annulus.

Extensive experimental investigations classifying flow patterns were conducted by Powe et al. (1969). They found that the free convective flow of air can be neatly categorized into four basic types depending upon the Grashop number (or Rayleigh number) and the inverse relative gap width σ (= diameter of the inner cylinder/gap width), and delineated different flow regimes (see Figure 8). For sufficiently small Rayleigh number, a steady 2-D flow with two crescent-shaped eddies symmetric with respect to the vertical plane through the common center of cylinders occurs regardless of σ. As the Rayleigh number was increased above a critical value, different unsteady flow patterns were observed, depending on σ: a 2-D oscillatory flow for $\sigma < 2.8$ (wide gap), a three-dimensional (3-D) spiral flow for $2.8 < \sigma < 8.5$ (medium-sized gap), and a 2-D multicellular flow for $\sigma > 8.5$ (narrow gap). Some values of the critical Rayleigh numbers were $Ra_{cr} \approx 7 \times 10^4$ for $\sigma = 2$; $Ra_{cr} \approx 2000$ for $\sigma = 4.76$; and $Ra_{cr} \approx 4900$ for $\sigma = 10$. More recently, Rao et al. (1985) carried out numerical and experimental investigations of flow pattern classification. The general trend was consistent with that of Powe et al., except for the case of wide annulus ($\sigma < 2.8$) in which they failed to realize the 2-D oscillatory flow numerically. For a narrow annulus ($\sigma > 8.5$), with increase of Ra, the steady unicellular flow pattern changed into a steady multicellular flow pattern when the Rayleigh number exceeded a critical value, and the further increase of the Rayleigh number created an oscillatory multicellular flow pattern.

Thermal convection of fluids with low Prandtl number such as liquid metals, exhibits more complicated flow patterns for high Rayleigh numbers (Mack and Bishop 1968; Custer and Shaughnessy 1977; Charrier-Mojtabi et al. 1979; Fant et al. 1990; Yoo et al. 1994). Especially, Fant et al. studied unsteady natural convection for the limiting case of $Pr = 0$. They simplified the Boussinesq approximated Navier–Stokes equations into Cartesian-like boundary-layer equations by means of a high Rayleigh number, small-gap asymptotic theory. They found that a steady multicellular instability sets in first, and then time-periodic and complex unsteady multicellular flows develop as the scaled gap spacing increases. Recently, Yoo et al. investigated the 2-D natural convection of a low Prandtl number ($Pr = 0.2$) fluid in a wide range of gap widths. They solved the complete 2-D Navier–Stokes equations and the energy equation without approximations, such as those of Fant et al. From the numerical experiment, Yoo et al. observed steady and oscillatory like-rotating multicellular flow patterns that originated from the hydrodynamic type of instability. The results were as follows. For low Grashof numbers, a steady unicellular convection was obtained. Above a transition Grashof number that depends on the gap width, a steady bicellular flow occurred. With further increase of the Grashof number, steady or time-periodic multicellular convection occurred. Finally, complex oscillatory multicellular flow appeared. They plotted the transition Grashoff number at which the types of flow patterns were altered as functions of inverse relative gap width σ and showed that the actual behavior of the oscillatory flow was different from the result of Fant et al., where some approximations were made.

In this numerical study, the present author reports that if the Rayleigh number based on the gap width is greater than a certain critical value, dual steady solutions are realized in the flow regime in which both Powe et al. (1969) and Rao et al. (1985) have confirmed that a steady 2-D flow prevails. When the Rayleigh number is small, the crescent-shaped eddy pattern

Address reprint requests to Prof. Joo-Sik Yoo, Department of Mechanical Engineering Education, Andong National University, 388 Songchun-Dong, Andong, Kyungpuk 760-749, South Korea.

Received 18 January 1996; accepted 18 May 1996

Int. J. Heat and Fluid Flow 17: 587–593, 1996

655 Avenue of the Americas, New York, NY 10010

0142-727X/96/$15.00
PII S0142-727X(96)00064-3

appears over the whole range of σ. However, if the Rayleigh number is larger than a critical value that depends on the gap width, two kinds of flow patterns are realized according to initial conditions: one is the commonly observed crescent-shaped pattern in which the fluid ascends along the central plane when the inner cylinder is kept hotter (designated as "upward" flow), and the other, the flow consisting of two counter-rotating eddies and their mirror image ("downward" flow) (see Figure 3). Although multiple steady solutions for several hydrodynamic problems (Taylor problem, Dean problem etc.) have been investigated experimentally and theoretically, (Yoo and Kim 1991; Zandbergen et al. 1987; Dennis and Ng 1982; Benjamin and Mullin 1982; Nandakumar et al. 1985) the existence of dual solutions for the natural convection in a horizontal annulus has never been reported in any of the numerical and/or experimental studies as far as the present author is aware.

The occurrence of dual steady states at a given Rayleigh number larger than a critical value can be regarded as an example of bifurcation phenomena. The distribution of local Nusselt number for "downward flow" is significantly different from that for "upward flow," especially in the upper region, as the buoyant plume separates at a point other than the top of the inner cylinder for "downward flow." However, the overall Nusselt number is little affected by the type of flows.

Analysis

The geometry of the problem and the coordinate system are shown in Figure 1. The fluid is contained between two infinite horizontal concentric circular cylinders, which are held at different uniform temperatures of T_i and T_o ($T_i > T_o$). Density change in the fluid is neglected everywhere except in the buoyancy, and all the other physical properties of the fluid are assumed constant (Boussinesq approximation). Viscous dissipation in the energy equation is also neglected. We use the cylindrical coordinates r, ϕ, the angular coordinate ϕ being measured counterclockwise from the upward vertical through the center of the cylinders. The equations governing conservation of mass, momentum and, energy are put into nondimensional form by taking the characteristic length, time, velocity, pressure, and temperature as $L(=R_o - R_i)$, L^2/κ, κ/L, $\rho_0\kappa^2/L^2$ and $(T_i - T_o)$, respectively. We let $\mathrm{Pr} = \nu/\kappa$ and $\mathrm{Ra} = \alpha g(T_i - T_o)L^3/\kappa\nu$ denote the Prandtl and Rayleigh numbers, respectively.

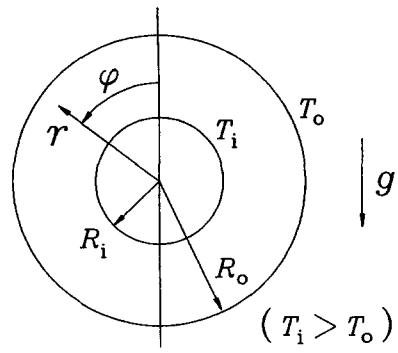

Figure 1 Problem configuration

The dimensionless equations governing the 2-D convection are

$$\frac{\partial \omega}{\partial t} = \mathrm{J}(\Psi, \omega) + \mathrm{Pr}\,\nabla^2\omega - \mathrm{PrRa}\left[\sin(\phi)\frac{\partial \theta}{\partial r} + \cos(\phi)\frac{\partial \theta}{r\partial \phi}\right] \quad (1)$$

$$\omega = -\nabla^2\Psi \quad (2)$$

$$\frac{\partial \theta}{\partial t} = \mathrm{J}(\Psi, \theta) + \nabla^2\theta \quad (3)$$

where the vorticity ω, streamfunction Ψ, Jacobian $\mathrm{J}(f,g)$ and Laplacian ∇^2 are

$$\omega = \frac{\partial}{r\partial r}(rv) - \frac{\partial}{r\partial \phi}(u), \qquad u = \frac{\partial \Psi}{r\partial \phi}, \qquad v = -\frac{\partial \Psi}{\partial r}$$

$$\mathrm{J}(f,g) = \frac{1}{r}\left(\frac{\partial f}{\partial r}\frac{\partial g}{\partial \phi} - \frac{\partial f}{\partial \phi}\frac{\partial g}{\partial r}\right)$$

$$\nabla^2 = \frac{\partial}{r\partial r}\left(r\frac{\partial}{\partial r}\right) + \frac{\partial^2}{r^2\partial \phi^2} \quad (4)$$

Notation

D_i	diameter of inner cylinder
g	acceleration of gravity
J	Jacobian
L	gap width of the annulus, $R_0 - R_i$
Nu	overall Nusselt number, $(\overline{\mathrm{Nu}_i} + \overline{\mathrm{Nu}_o})/2$
$\mathrm{Nu}_{\mathrm{cond}}$	Nusselt number of pure conduction state
$\mathrm{Nu}_i, \mathrm{Nu}_o$	local Nusselt numbers at the inner and outer cylinders, respectively
$\overline{\mathrm{Nu}_i}, \overline{\mathrm{Nu}_o}$	mean Nusselt numbers at the inner and outer cylinders, respectively
Pr	Prandtl number, ν/κ
R_i, R_o	radii of the inner and outer cylinders, respectively
Ra	Rayleigh number based on the gap width, $\alpha g(T_i - T_o)L^3/\kappa\nu$
r_i, r_o	dimensionless radii of the inner and outer cylinders, respectively, $r_i = R_i/L(=\sigma/2)$, $r_o = R_o/L(=1+\sigma/2)$
t	dimensionless time
T_i, T_o	temperatures at the inner and the outer cylinders, respectively

Greek

α	coefficient of thermal expansion
η	stretched coordinate in the radial direction
θ	dimensionless temperature
κ	thermal diffusivity
ν	kinematic viscosity
ρ_0	mean density
σ	ratio of the inner cylinder diameter to gap width, D_i/L
ϕ	azimuthal coordinate
ϕ_S	angle locating the separation point between two rolls in the "downward" flow, Figure 3b
ψ	dimensionless stream function
ω	dimensionless vorticity

The boundary conditions on the two walls are

$$\Psi = \frac{\partial \Psi}{\partial r} = 0, \qquad \omega = -\frac{\partial^2 \Psi}{\partial r^2}, \qquad \theta = 1 \quad \text{at} \quad r = r_i \tag{5}$$

$$\Psi = \frac{\partial \Psi}{\partial r} = 0, \qquad \omega = -\frac{\partial^2 \Psi}{\partial r^2}, \qquad \theta = 0 \quad \text{at} \quad r = r_o \tag{6}$$

We impose following symmetric conditions

$$\Psi = \omega = \frac{\partial^2 \Psi}{\partial \phi^2} = \frac{\partial \theta}{\partial \phi} = 0 \quad \text{at} \quad \phi = 0, \pi \tag{7}$$

because we suppose the flow to be symmetric with respect to the vertical plane through the center of cylinders.

The dimensionless heat transfer rate of pure conduction in the absence of fluid motion is

$$\mathrm{Nu}_{\mathrm{cond}} = \frac{1}{\ln(r_o/r_i)} \tag{8}$$

The local Nusselt number is defined as the actual heat flux divided by $\mathrm{Nu}_{\mathrm{cond}}$,

$$\mathrm{Nu}_i(\phi) = -\left(r\frac{\partial \theta}{\partial r}\right)\Big/ \mathrm{Nu}_{\mathrm{cond}} \quad \text{at} \quad r = r_i \tag{9}$$

$$\mathrm{Nu}_o(\phi) = -\left(r\frac{\partial \theta}{\partial r}\right)\Big/ \mathrm{Nu}_{\mathrm{cond}} \quad \text{at} \quad r = r_0 \tag{10}$$

and the mean Nusselt numbers $\overline{\mathrm{Nu}_i}$ and $\overline{\mathrm{Nu}_o}$ are given by

$$\overline{\mathrm{Nu}_i} = \frac{1}{\pi}\int_0^{\pi} \mathrm{Nu}_i(\phi)\, d\phi \tag{11}$$

$$\overline{\mathrm{Nu}_o} = \frac{1}{\pi}\int_0^{\pi} \mathrm{Nu}_o(\phi)\, d\phi \tag{12}$$

In steady states, $\overline{\mathrm{Nu}_i}$ and $\overline{\mathrm{Nu}_o}$ are presumably of the same value.

Equations 1–7 are solved numerically, by the same finite difference method used in Yoo et al. (1994) and Yoo and Kim (1991). Equations 1 and 3 are cast into finite difference form using the leap-frog method (Roache 1972) of Dufort-Frankel for the diffusion and time derivative terms, with central differencing for the Jacobian. The Poisson equation, Equation 2, for the stream function is discretized by use of five-point formula. Because the computational domain is rectangular, the discretized Poisson equation is solved by the direct method of Buzbee et al. (1970), which uses cyclic even–odd reduction method. The algorithm of Buzbee et al. is known to be extremely fast and accurate. In the azimuthal direction, a uniform grid is employed, and in the radial direction, the following coordinate stretching is utilized.

$$r = r_i + \frac{1}{2}\left\{1 + \frac{\tanh[C(2\eta - 1)]}{\tanh(C)}\right\} \quad \text{with } C = 1.5 \qquad 0 \le \eta \le 1 \tag{13}$$

The solution was considered to have converged to the steady state, when the absolute value of the maximum relative difference between two consecutive time steps was less than a prescribed value ε:

$$\mathrm{Max}\left|\frac{f_{i,j}^{n+1} - f_{i,j}^{n}}{f_{i,j}^{n+1}}\right| < \varepsilon \quad \text{for} \quad f = \omega, \Psi \text{ and } \theta \tag{14}$$

For most cases, ε was set equal to 10^{-5}, but computation was often continued until $\varepsilon = 10^{-10}$ to be sure that the steady downward flow really persists. The time step Δt was taken in the range of $10^{-5} < \Delta t < 10^{-2}$. At the initial stage, a small time step $\Delta t \simeq 10^{-5}$ was used, and later on Δt was changed to a larger value $\Delta t \simeq 10^{-3}$. According to the values of inverse relative gap width σ, different grids were used: (55×65) for $\sigma < 2$; (35×33) for $\sigma = 2, 3$; (21×65) for $\sigma = 4$; and (17×129) for $\sigma = 6, 8, 10$.

Results and Discussion

To check the numerical scheme, the mean Nusselt number is compared with that of Kuehn and Goldstein (1976) at $\mathrm{Ra} = 10^4$ for various values of σ. The result shows good agreement with that of Kuehn and Goldstein except in the case of $\sigma = 10$ (Table 1). The discrepancy is most certainly due to the coarse mesh (16×19) adopted by Kuehn and Goldstein, because the present method obtained the mean Nusselt numbers $\overline{\mathrm{Nu}_i} = 1.271$ and $\overline{\mathrm{Nu}_o} = 1.274$ with (16×17) grid.

Computations were performed for various combinations of Ra and σ in the range of $10^3 \le \mathrm{Ra} \le 2 \times 10^5$ and $0.1 \le \sigma \le 10$, for a Prandtl number of 0.7(air). A series of numerical calculations was set out by choosing a large value of Ra after having fixed σ. The system of Equations 1–3 was integrated with initial conditions of $\psi = \omega = 0$ and $\theta = 1$ throughout the entire region, until a converged steady solution was obtained. In the case of a not large σ ($\sigma < 6$), artificial numerical disturbances were introduced during a short initial period ($t \lesssim 0.01$), to enhance the separation of boundary layer from a point other than the top of inner cylinder. Once having obtained the steady "downward" flow, the Rayleigh number was decreased, and the steady solution was found by letting the initial conditions be the steady solution previously obtained, to save the computation time. This process was carried out successively until only the "upward" flow was realized (down-scan). Then, with increase of Ra (up-scan), steady solutions for the same Rayleigh numbers as down-scan stage were obtained. All the steady solutions at up-scan stage were found to be "upward" flows (see Figure 2).

Firstly, the results for $\sigma = 1.25$, an annulus with a wide gap, is presented. Dual steady solutions are observed when the Rayleigh number is larger than a critical value $\mathrm{Ra}_{\mathrm{cr}}$ about 3800, and for $\mathrm{Ra} < \mathrm{Ra}_{\mathrm{cr}}$, only the crescent-shaped flow is realized, regardless of the initial condition. A few streamlines and isotherms are depicted in Figure 3. As shown in the figure, the "downward" flow consists of a small counter-rotating eddy in the top region of the gap sitting above a large one. The small eddy is approximately square-shaped, and the size is not much affected by Ra. The value of $|\psi_{\mathrm{min}}|$, which may be considered as a measure of the

Table 1 Comparison of Nusselt numbers with those of Kuehn and Goldstein (1976) at Ra = 10,000

σ	Present $\overline{\mathrm{Nu}_i}, \overline{\mathrm{Nu}_o}$	Kuehn and Goldstein (1976) $\overline{\mathrm{Nu}_i}, \overline{\mathrm{Nu}_o}$
0.125	(1.835, 1.922)	(1.878, 2.051)
0.5	(2.082, 2.109)	(2.148, 2.157)
1.0	(2.022, 2.037)	(2.061, 2.059)
1.25	(1.973, 1.985)	(2.010, 2.005)
2.0	(1.837, 1.848)	(1.850, 1.853)
10.0	(1.562, 1.567)	(1.271, 1.276)

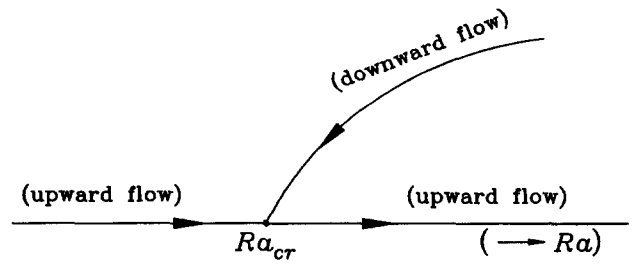

Figure 2 Bifurcation diagram for the "downward" and "upward" flows; the transition from "upward" to "downward" flow does not occur; only a transition from "downward" to "upward" flow occurs at $Ra = Ra_{cr}$

strength of the small counter-rotating eddy, diminishes rapidly as the Rayleigh number decreases to the critical value Ra_{cr} (Figure 4). For "downward" flow, the point of ψ_{max} (indicated by the cross), which would be the center of rotation of large eddy, moves slightly upwards as the Rayleigh number increases, but stays near $\phi = 90°$ when the Rayleigh number is not much larger than Ra_{cr}. The temperature distribution of "downward" flow differs significantly from that of "upward" flow, especially in the top region. Figure 5 shows the distribution of local Nusselt numbers for the inner and outer cylinders at two values of Ra. Although the distribution of local Nusselt numbers for "upward" and "downward" flows are significantly different from each other

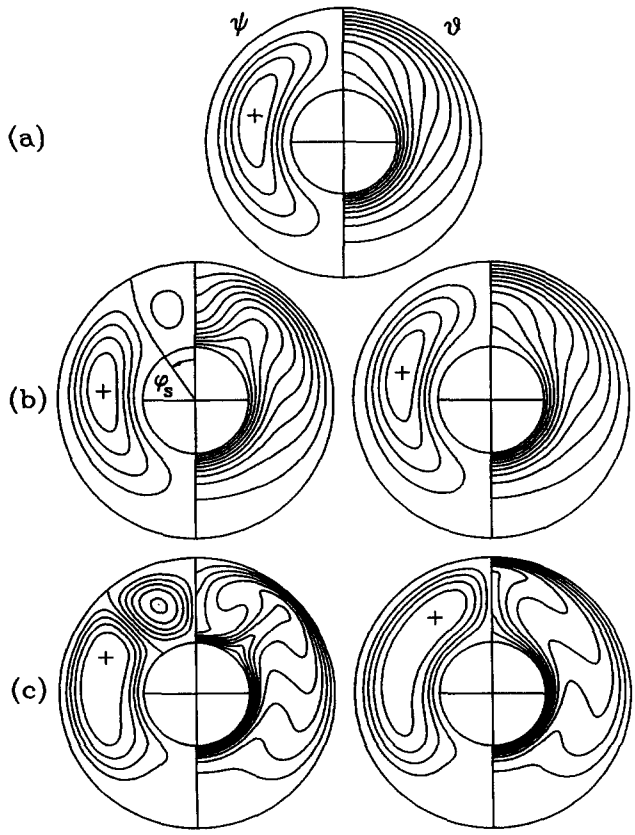

Figure 3 Streamlines and isotherms when $\sigma = 1.25$; the left are downward flows and the right are upward flows: (a) Ra=3000; (b) Ra=4000; (c) Ra=50,000; the streamlines and isotherms of upward flows are similar to those given by Kuehn and Goldstein (1976)

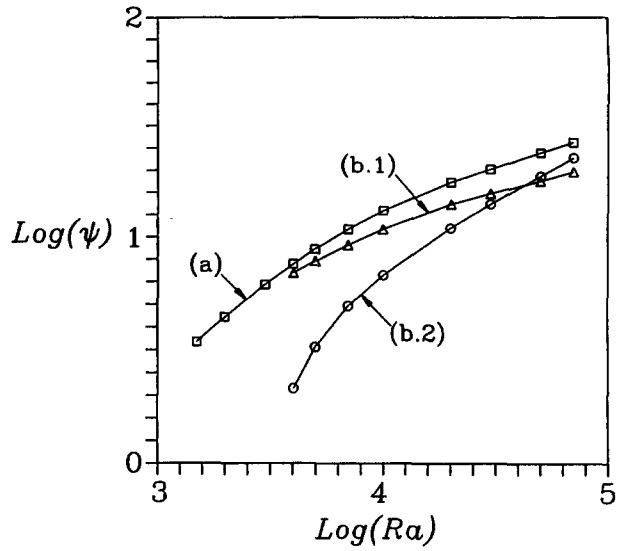

Figure 4 Maximum and minimum values of stream function as a function of Rayleigh number when $\sigma = 1.25$: (a) ψ_{max} of upward flow; (b.1) ψ_{max} of downward flow; (b.2) $-\psi_{min}$ of downward flow

except at the bottom region, the difference in overall Nusselt numbers is rather small; Nu for "downward" flow is larger than that for "upward" flow within 9%.

For an annulus with a medium-sized gap ($2.8 < \sigma < 8.5$), the features of steady solutions are similar to those for a wide gap. Plots of streamlines and isotherms are given in Figure 6, for $\sigma = 4$ and Ra = 3000, a value near the critical Rayleigh number.

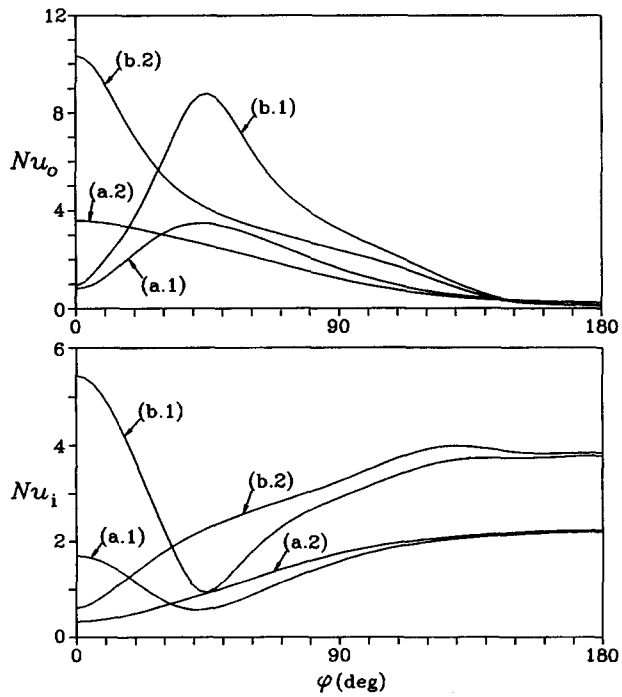

Figure 5 Distribution of local Nusselt numbers at the inner and outer cylinders with $\sigma = 1.25$ when Ra=4000 (a.1, a.2) and Ra=50,000 (b.1, b.2); (a.1) and (b.1) downward flow; (a.2) and (b.2) upward flow

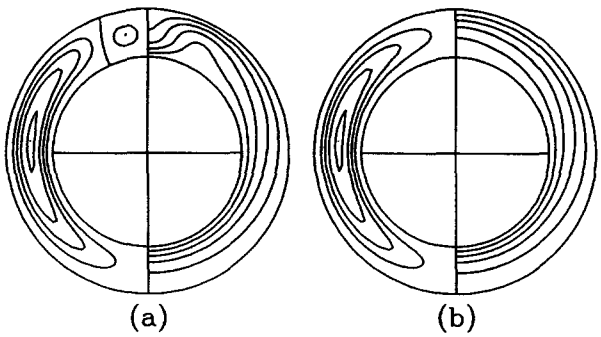

Figure 6 Streamlines and isotherms when $\sigma=4$ and Ra= 3000; (a) downward flow, (b) upward flow

For $\sigma = 10$ (narrow annulus), both types of the flow are realized when the Rayleigh number is larger than a critical value about 1900, below which only "upward" flow of a crescent-shaped eddy pattern appears. As the Rayleigh number exceeds another transition Rayleigh number of about 3000, crescent-shaped "upward" flow changes into a steady multicellular flow (Figure 7b), consistent with the results of Rao et al. (1985), and the flow remains steady up to $Ra \approx 10^4$. "Downward" flow persists, even in the range in which a steady multicellular flow is observed. Streamlines and isotherms are illustrated in Figure 7.

In the present numerical study, dual steady solutions were found for $\sigma \geq 0.3$. When $\sigma = 0.2$, "downward" flow was not realized even at very large Rayleigh number ($Ra = 2 \times 10^5$), although the steady "downward" flow for $\sigma = 0.3$ was used as the initial value. In a short initial period, the eddy in the top region subsided, and the commonly observed crescent-shaped flow was established. The critical Rayleigh number above which dual steady solutions exist rapidly decreases as the inverse relative gap width σ increases, and tends to a finite limit as $\sigma \to \infty$ (Figure 8). The limiting value is conjectured to be 1708, because the flow at the top region of a very narrow annulus ($\sigma \gg 1$) can be approximated as the convection between two horizontal planes heated from below (Bénard convection). In Figure 8, dashed lines reproduced from the experimental work of Powe et al. (1969) indicate the transition Rayleigh number below which a steady two-dimensional flow prevails.

In the "downward" flow, this study defines ϕ_S as the angle representing the location of the separation point between the two rolls (see Figure 3b). The size of the counter-rotating eddy in the top region can be estimated by ϕ_S at the inner and outer cylinders. Some values of ϕ_S as a function of σ and Ra are given

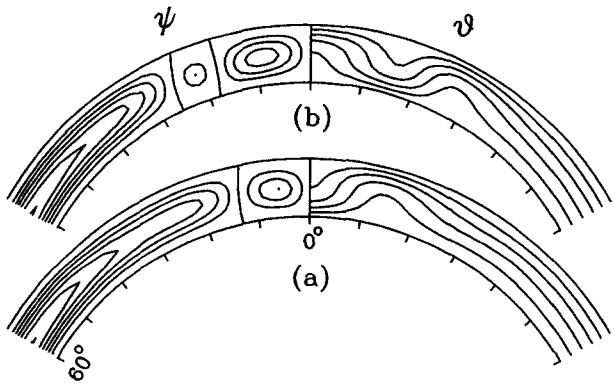

Figure 7 Streamlines and isotherms when $\sigma=10$: (a) downward flow with Ra=2000; (b) multicellular upward flow with Ra=3000

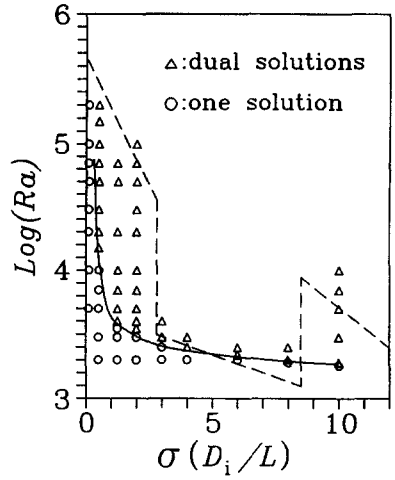

Figure 8 Map of the downward and upward flows on the Ra-σ plane; (o=only upward flow exists); (Δ=two flows are coexisting); continuous line represents the critical Rayleigh number ($Ra = Ra_{cr}$) above which dual steady solutions exist; dashed lines reproduced from the experimental work of Powe et al. (1969) indicate the transition Rayleigh number below which a steady 2-D flow prevails

in Table 2. In general, the counter-rotating eddy is approximately square-shaped. ϕ_S is increased as σ decreases. However, it does not exceed $\pi/4$ at the inner cylinder where the hot region of $\phi > \phi_S$ drives the fluid upward. For $\sigma = 0.5$ and 2, ϕ_S is not much affected by Ra. Figure 9 illustrates the locations of the

Table 2 Angles (ϕ_S) locating the separation points between two rolls in the "downward" flow (see Figure 3b)

σ	Ra	ϕ_S (inner, outer)
0.3	100,000	(36.9, 49.4)
0.5	15,000	(39.5, 39.7)
0.5	20,000	(41.0, 41.9)
0.5	30,000	(41.8, 44.1)
0.5	50,000	(42.3, 46.2)
0.5	100,000	(43.0, 48.4)
0.5	200,000	(43.1, 50.0)
0.7	20,000	(43.6, 42.2)
1.0	20,000	(42.5, 41.0)
2.0	3500	(32.0, 25.1)
2.0	5000	(36.7, 29.4)
2.0	10,000	(38.6, 33.9)
2.0	20,000	(37.1, 36.0)
2.0	50,000	(33.3, 36.3)
2.0	100,000	(31.3, 35.6)
4.0	2500	(20.7, 17.5)
6.0	2200	(15.4, 13.6)
8.0	2000	(11.0, 10.1)
10.0	1900	(7.4, 6.9)
10.0	2000	(9.6, 8.9)
10.0	3000	(13.2, 11.9)
10.0	5000	(16.6, 14.7)
10.0	7000	(18.9, 16.4)
10.0	10,000	(21.4, 18.2)

The unit of ϕ_S is degree; the terms "inner" and "outer" represent the inner and outer cylinders, respectively

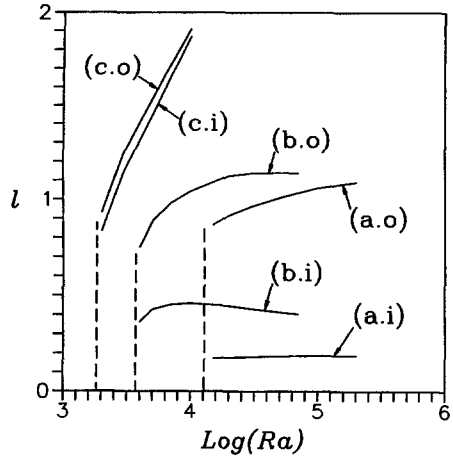

Figure 9 Location of the separating streamline of downward flow measured by the arc length l from the top ($\phi=0$): (a) $\sigma=0.5$; (b) $\sigma=1.25$; (c) $\sigma=10$; the letters "i" and "o" denote the inner and outer cylinders, respectively

separating streamline at the inner and outer cylinders as measured by arc lengths from the top as functions of Ra for $\sigma = 0.5, 1.25, 10$.

The overall Nusselt numbers are shown in Figure 10 as functions of Rayleigh number. For a very wide annulus ($\sigma \lesssim 0.7$), Nu for "upward" flow is found slightly larger than that for "downward" flow, but the opposite tendency has been observed for $1 \lesssim \sigma \lesssim 8.5$.

To examine the process to steady "downward" flow from an initially quiescent and isothermal state, the transient development of flow patterns and isotherms for $\sigma = 6$, when the outer surface is suddenly cooled to $Ra = 10^4$ is presented in Figure 11. At the very early time ($t = 0.01$), a prominent roll is created with the center near the outer cylinder and $\phi \approx 90°$ (Figure 11a). The physical mechanism responsible for the creation of the roll is obvious: when the density (temperature) gradient has a component orthogonal to gravitational field, the fluid motion sets in, however small the component is. As the time elapses ($t \lesssim 0.15$), the center of roll descends, and an unstably stratified stagnant region near the top expands (Figure 11b). After a while, the center ascends, and the boundary layer adjacent to the inner

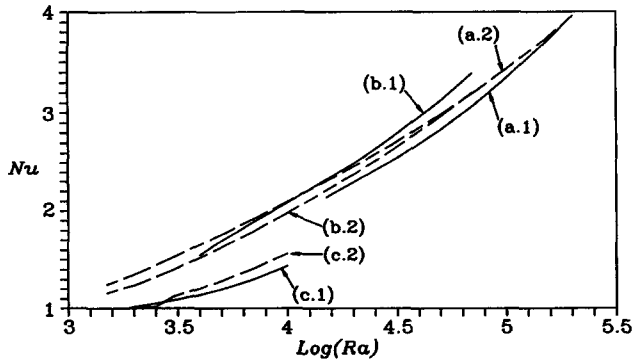

Figure 10 Overall Nusselt numbers as a function of Rayleigh number for $\sigma=0.5$ (a), 1.25 (b), and 10 (c); letters "1" and "2" denote downward and upward flows, respectively

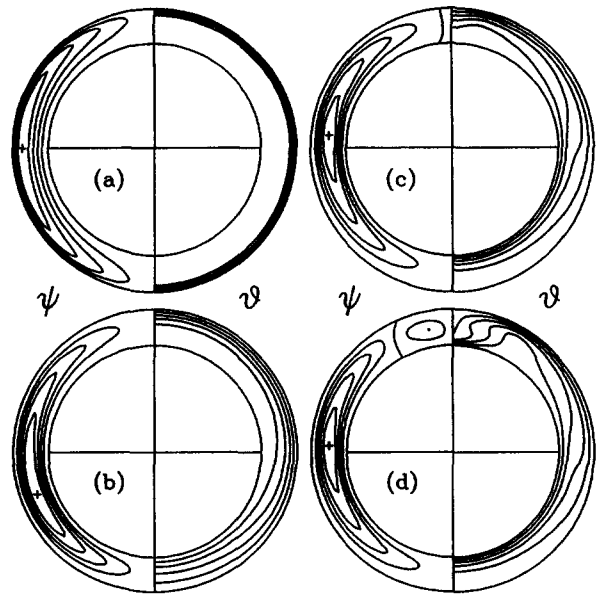

Figure 11 Transient development of flow patterns and isotherms for $\sigma=6$ and $Ra=10{,}000$ when the outer cylinder is suddenly cooled; the initial conditions are $\psi=\omega=0$ and $\theta=1$, and the outer cylinder is suddenly cooled to $\theta=0$: (a) $t=0.01$; (b) $t=0.11$; (c) $t=1.06$; (d) steady state

cylinder separates at a point other than the top, and a slim counter-rotating eddy is formed in the thermally unstable region (Figure 11c). The eddy formed in the top region gradually expands, and a steady motion consisted with two counter-rotating eddies ("downward" flow) is established (Figure 11d). For the purpose of comparison, the transient development of flow pat-

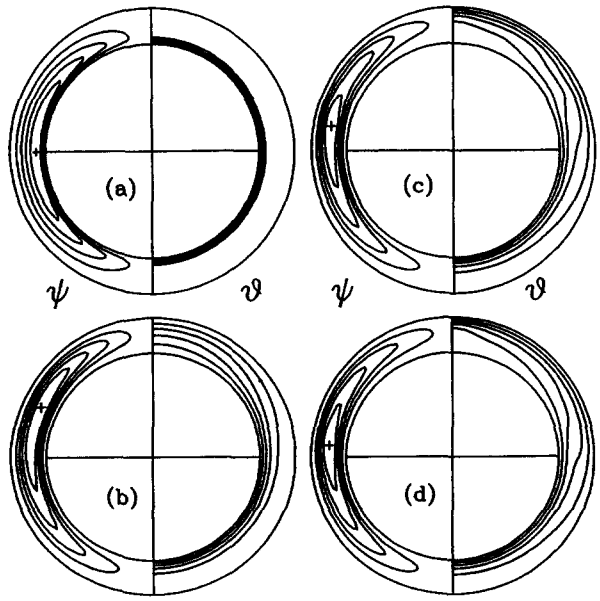

Figure 12 Transient development of flow patterns and isotherms for $\sigma=6$ and $Ra=10{,}000$ when the inner cylinder is suddenly heated; the initial conditions are $\theta=\psi=\omega=0$, and the inner cylinder is suddenly heated to $\theta=1$: (a) $t=0.01$; (b) $t=0.11$; (c) $t=1.06$; (d) steady state

terns and isotherms for the same Rayleigh number ($Ra = 10^4$), when the inner cylinder is suddenly heated to $Ra = 10^4$ from an isothermal quiescent state ($\theta = \psi = \omega = 0$) is presented in Figure 12. The results agree qualitatively with those by Casterejon and Spalding (1988). In steady state, the streamlines are of crescent-shaped eddy pattern.

For the occurrence of "downward" flow, it seems necessary that the boundary layer on the inner cylinder separates at a point other than the top of the cylinder to trigger an eddy in the thermally unstable top region. Once a small eddy has been triggered, the eddy grows and finally "downward" flow consisting of two counter-rotating eddies develops, if the unstable stratification in the top region is sufficiently strong. For a narrow annulus in which the radius of curvature is large, the boundary layer on the inner cylinder is more likely to separate at a point other than the top. It is also to be noted that "downward" flow has not been obtained in the present numerical experiment, when "upward" flow is used as the initial condition. This implies that once "upward' flow has been established, "downward" flow cannot be obtained by changing the Rayleigh number. Only the transition from "downward" to "upward" flow occurs at $Ra = Ra_{cr}$.

References

Benjamin, T. B. and Mullin, T. 1982. Notes on the multiplicity of flows in the Taylor experiment, *J. Fluid Mech.*, **121**, 219–230

Buzbee, B. L., Golub, G. H. and Nielson, C. W. 1970. On direct methods for solving Poisson's Equations. *SIAM J. Numer. Anal.*, 7, 627–656

Castrejon, A. and Spalding, D. B. 1988. An experimental and theoretical study of transient free-convection flow between horizontal concentric cylinders. *Int. J. Heat Mass Transfer* **31**, 273–284

Charrier-Mojtabi, M. C., Mojtabi, A. and Caltagirone, J. P. 1979. Numerical solution of a flow due to natural convection in horizontal cylindrical annulus. *J. Heat Transfer*, **101**, 171–173

Custer, J. R. and Shaughnessy, E. J. 1977. Thermoconvective motion of low Prandtl number fluids within a horizontal cylindrical annulus. *J. Heat Transfer*, **99**, 596–602

Dennis, S. C. R. and Ng, M. 1982. Dual solutions for steady laminar flow through a curved tube, *Quarterly J. Mech. Appl. Math.*, **35**, 305–324

Fant, D. B., Prusa, J. and Rothmayer, A. P. 1990. Unsteady multicellular natural convection in a narrow horizontal cylindrical annulus. *J. Heat Transfer*, **112**, 379–387

Kuehn, T. H. and Goldstein, R. J. 1976. An experimental and theoretical study of natural convection in the annulus between horizontal concentric cylinders. *J. Fluid Mech.*, **74**, 695–719

Mack, L. R. and Bishop, E. H. 1968. Natural convection between horizontal concentric cylinders for low Rayleigh numbers. *Quarterly J. Mech. Appl. Math.* **21**, 223–241

Nandakumar, K., Masliyah, J. H. and Law, H. S. 1985. Bifurcation in steady laminar mixed convection flow in horizontal ducts. *J. Fluid Mech.*, **152**, 145–161

Powe, R. E., Carley, C. T. and Bishop, E. H. 1969. Free convective flow patterns in cylindrical annuli. *J. Heat Transfer*, **91**, 310–314

Rao, Y. E., Miki, Y., Fukuda, K., Yakata, Y. and Hasegawa, S. 1985. Flow patterns of natural convection in horizontal annuli. *Int. J. Heat Mass Transfer*, **28**, 705–714

Roache, P. J., 1972. *Computational Fluid Dynamics*. Hermosa.

Yoo, J. S., Choi, J. Y. and Kim, M. U. 1994. Multicellular natural convection of a low Prandtl number fluid between horizontal concentric cylinders. *Numer. Heat Transfer Part A*, **25**, 103–115

Yoo, J. S. and Kim, M. U. 1991. Two-dimensional convection in a horizontal fluid layer with spatially periodic boundary temperatures. *Fluid. Dyn. Res.* **7**, 181–200.

Zandbergen, P. J. and Dijkstra, D. 1987. Von-Kármán swirling flows. *Ann. Rev. Fluid Mech.*, **19**, 465–491